Title

Evidence for a delocalization quantum phase transition without symmetry breaking in CeCoIn5

Journal

Science, 375(6576)

ISSN

0036-8075

Authors

Maksimovic, Nikola
Eilbott, Daniel H
Cookmeyer, Tessa
et al.

Publication Date

2022-01-07

DOI

10.1126/science.aaz4566

Peer reviewed

HEAVY FERMIONS

Evidence for a delocalization quantum phase transition without symmetry breaking in $CeCoIn_5$

Nikola Maksimovic[1,2]*, Daniel H. Eilbott[1,2], Tessa Cookmeyer[1,2], Fanghui Wan[1,2], Jan Rusz[3], Vikram Nagarajan[1,2], Shannon C. Haley[1,2], Eran Maniv[1,2], Amanda Gong[1,2], Stefano Faubel[1,2], Ian M. Hayes[1,2], Ali Bangura[4], John Singleton[5], Johanna C. Palmstrom[5], Laurel Winter[5], Ross McDonald[5], Sooyoung Jang[1,2], Ping Ai[2], Yi Lin[2], Samuel Ciocys[1,2], Jacob Gobbo[1,2], Yochai Werman[1,2], Peter M. Oppeneer[3], Ehud Altman[1,2], Alessandra Lanzara[1,2], James G. Analytis[1,2]*

The study of quantum phase transitions that are not clearly associated with broken symmetry is a major effort in condensed matter physics, particularly in regard to the problem of high-temperature superconductivity, for which such transitions are thought to underlie the mechanism of superconductivity itself. Here we argue that the putative quantum critical point in the prototypical unconventional superconductor $CeCoIn_5$ is characterized by the delocalization of electrons in a transition that connects two Fermi surfaces of different volumes, with no apparent broken symmetry. Drawing on established theory of f-electron metals, we discuss an interpretation for such a transition that involves the fractionalization of spin and charge, a model that effectively describes the anomalous transport behavior we measured for the Hall effect.

$CeCoIn_5$ is an f-electron metal with notable similarities to high-temperature superconducting copper oxides, for example, in crystal structure, transport properties, and unconventional superconductivity (*1*–*10*). Both $CeCoIn_5$ and this category of copper oxides also exhibit signatures of a quantum phase transition (QPT), a phase transition induced by a nonthermal parameter, underlying the superconducting state. However, in many unconventional superconductors, it is unclear whether the underlying QPT can be understood in the conventional sense as a process of separating phases with different symmetries. Unconventional types of QPTs, such as non–symmetry breaking (*11*) or weakly symmetry breaking (*12*, *13*) QPTs, have therefore become a subject of intense study. In this work, we provide evidence that $CeCoIn_5$ is proximate to a QPT in which the density of itinerant electrons changes, apparently without the breaking of symmetry. Established theory of f-electron metals provides a means to interpret such a transition.

At the microscopic level, f-electron metals such as $CeCoIn_5$ are described by a Kondo lattice model. Each Ce atom hosts a single f-level valence electron, which contributes a localized spin-½ moment. These local moments coexist with a sea of itinerant conduction electrons. In the conventional metallic ground state of the Kondo lattice, the f-electrons appear to become an integral part of the itinerant metal. In particular, they join the conduction electrons, contributing their full share to the total Fermi volume as prescribed by Luttinger's theorem (*14*). This phenomenon occurs through the formation of Kondo singlet correlations between the local f moments and the conduction electrons, which effectively hybridize the f level with the conduction bands.

A long-standing challenge has been to characterize a QPT in which the f electrons recover their localized character and withdraw from the itinerant Fermi volume. Superficially, the remaining Fermi volume without f electrons is in apparent violation of Luttinger's theorem. The loss of Fermi volume when f electrons localize is therefore conventionally accompanied by a transition to a spin-density wave state, whereby Luttinger's theorem is recovered in the appropriately folded Brillouin zone associated with translational symmetry breaking (*15*–*19*). In this paper, we present Hall effect, quantum oscillation, and angle-resolved photoemission spectroscopy (ARPES) measurements of $CeCoIn_5$ with small levels of chemical substitution and compare the experimental data to ab initio calculations. We find evidence for an f-electron delocalization QPT without symmetry breaking.

Figure 1A presents low-temperature measurements of the Hall resistivity, ρ_{xy}, versus magnetic field, $\mu_0 H$, for $CeCoIn_5$ samples with varying levels of Cd (hole doping) or Sn (electron doping), both of which substitute In. The Hall coefficient, $R_H = \rho_{xy}/\mu_0 H$, can be used to estimate the net carrier density enclosed by the Fermi surface according to the formula (*20*)

$$n_{net} = \frac{1}{eR_H(H \to \infty)} \quad (1)$$

where n_{net} is the net carrier density—i.e., the carrier density of electrons minus that of holes. In multiple-band metals such as $CeCoIn_5$, Eq. 1 applies only in the limit where high fields eliminate the effects of carrier mobility imbalances and R_H becomes field independent [see section 3 of (*21*) for more details on the high-field limit]. For each sample, we measured the high-field value of R_H at 0.5 K to approximate the net carrier density. Many of the traces shown in Fig. 1A appear to saturate at high fields, and fig. S4 shows that the high-field slope of ρ_{xy} is in good agreement with the high-field value of $\rho_{xy}/\mu_0 H$, which suggests that, at these temperatures and fields, the Hall coefficient is nearly field independent. In addition, select samples were measured in pulsed magnetic fields up to 75 T, as shown in Fig. 1B, where the Hall coefficient is field independent over an extended field range; the extracted Hall coefficients from pulsed and continuous fields are in good agreement for these samples (Fig. 1C). Finally, our Hall coefficient measurements on pure $CeCoIn_5$ are consistent with measurements at 20 mK, at which the Hall resistivity is completely linear in field (*22*). Together, these findings provide evidence that our extracted Hall coefficient values can be interpreted as an approximate measurement of the net carrier density as described by Eq. 1.

Figure 1C shows the value of $1/eR_H$, approximating the net carrier density, extracted for samples with different levels of chemical substitution in continuous and pulsed magnetic fields. The carrier density of these material, excluding the f electron, can be established by using Hall resistivity measurements of $LaCoIn_5$ (Fig. 1B) (its Hall coefficient is field independent above 5 T at 1.8 K; see also fig. S3)—$LaCoIn_5$ can be thought of as $CeCoIn_5$ without the f electron. We find that the Hall coefficient of $CeCoIn_5$, evaluated either up to 60 T or up to 14 T at 0.5 K, is close to that of $LaCoIn_5$ (Fig. 1C). This suggests that the two materials have similar net carrier densities, implying that the f electrons are nearly localized in $CeCoIn_5$. With Cd substitution, $1/eR_H$ remains close to that of $LaCoIn_5$, but with Sn substitution it increases to a value consistent with the addition of one itinerant electron per unit cell. Identifying the additional electron as the single Ce f electron suggests that Sn substitution induces a delocalization transition of the f electrons. None of these samples show a finite-temperature phase transition other than that associated with superconductivity. Only when Cd-substitution levels exceed 0.6% is an antiferromagnetic phase observed (fig. S1) (*23*). In addition, the specific heat capacity at moderate temperature remains constant across this substitution series (Fig. 1C); we will comment more on this later.

[1]Department of Physics, University of California, Berkeley, Berkeley, CA 94720, USA. [2]Materials Sciences Division, Lawrence Berkeley National Laboratory, Berkeley, CA 94720, USA. [3]Department of Physics and Astronomy, Uppsala University, Box 516, S-75120 Uppsala, Sweden. [4]National High Magnetic Field Laboratory, Tallahassee, FL 32310, USA. [5]National High Magnetic Field Laboratory, Los Alamos, NM 97545, USA.
*Corresponding author. Email: nikola_maksimovic@berkeley.edu (N.M.); analytis@berkeley.edu (J.G.A.)

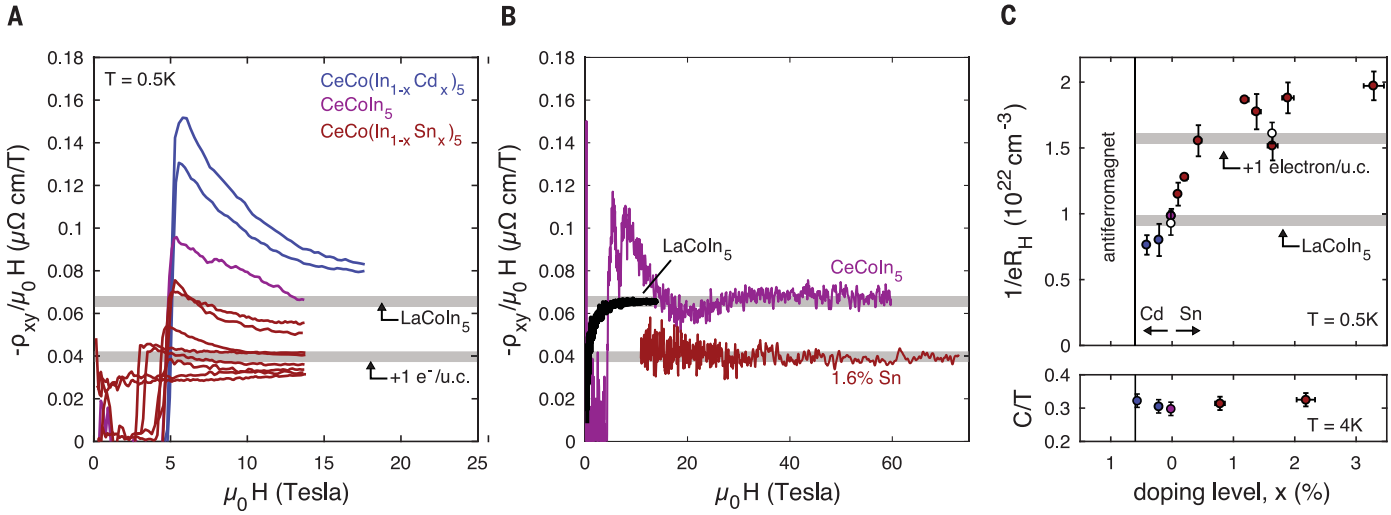

Fig. 1. Carrier density measurements in doped $CeCoIn_5$. (**A**) Hall coefficient as a function of field in doped $CeCoIn_5$ with Cd concentrations 0.2 and 0.4% and Sn concentrations 0.11, 0.22, 0.33, 0.44, 1.2, 1.39, 1.65, 1.9, and 3.3%. As discussed in the main text, the inverse of the Hall coefficient $\left(\rho_{xy}/\mu_0 H\right)$ in the high-field limit can be used to approximate the net carrier density [see also section 4 of (*21*)]. Gray lines denote the high-field Hall coefficient of the non-f analog $LaCoIn_5$ and the calculated value including one additional electron (e^-) per unit cell (u.c.). μΩ, microhm. (**B**) Pulsed-field Hall resistivity of $CeCoIn_5$ (T = 0.66 K) and Sn-doped $CeCoIn_5$ (T = 0.5 K) overlaid on the continuous-field Hall resistivity of $LaCoIn_5$ (1.8 K). (**C**) Inverse high-field Hall coefficient of $CeCoIn_5$ at 0.5 K as a function of doping level, including measurements in continuous field up to 14 or 18 T (filled circles) and pulsed field up to 73 T (open circles). With Sn substitution, the apparent carrier density of $CeCoIn_5$ increases by about one electron per unit cell above that of $LaCoIn_5$. This trend provides evidence that Sn substitution delocalizes the single Ce f electron per unit cell in $CeCoIn_5$. The value of $1/eR_H$ in some Sn-doped samples lies above the calculated +1 electron line, likely because the Hall coefficient has not completely saturated in these samples at 14 T. At higher fields, the value of $1/eR_H$ seems to saturate at the +1 electron value, as seen in the 1.6% Sn-doped sample at 70 T. The lower panel shows the 4 K heat capacity (units of millijoules per mole kelvin squared) across this doping series. Error bars indicate uncertainties in measurement of geometrical factors (in the case of the Hall resistivity) and sample mass (in the case of heat capacity).

When the f electrons delocalize, the Fermi surfaces are expected to reconstruct and increase in volume. The results of our density functional theory (DFT) calculations of the three Fermi surfaces to compare the (de) localized f-electron models are visualized in Fig. 2A [DFT calculation details are provided in section 1 of (*21*)]. According to the calculations, f-electron delocalization causes the extended γ surface to disconnect into small ellipsoidal pockets at the Brillouin zone center and edge and results in the disappearance of the γ pocket at the zone top (γ_Z). Also, large extended surfaces α_Z and β_Z appear at the zone top, and the α and β cylinders expand slightly. In pure $CeCoIn_5$, previous ARPES data at 10 to 20 K are in better qualitative agreement with the localized f-electron model, as α_Z and β_Z are absent and γ_Z is present (*24*, *25*). However, the volumes of the α and β cylinders are slightly larger than those of the localized model (*24*–*26*), and the smaller γ Fermi surface seems to exhibit features of both the delocalized and localized models: They are potentially disconnected (which suggests delocalization), but they retain γ_Z (indicative of localization) (*24*, *25*, *27*, *28*). These characteristics may point to a partially delocalized f-electron character in pure $CeCoIn_5$. This interpretation is also promoted by previous magnetic resonance (*29*) and photoemission (*24*, *30*, *31*) studies. Notably, our Hall effect measurements suggest that the f electrons only weakly contribute to the Fermi volume of $CeCoIn_5$, even at 0.5 K, consistent with the presence of partially localized f electrons in the low-temperature limit.

De Haas–van Alphen (dHvA) oscillations measure extremal areas of the Fermi surface perpendicular to the field direction, thus enabling examination of the Fermi surface structure at extremely low temperature. Here we compare our dHvA measurements of Sn-doped $CeCoIn_5$ and published data on pure $CeCoIn_5$ (*5*). As seen in Table 1 and Fig. 1C, the sizes of the α and β cylinder orbits in pure $CeCoIn_5$ are more consistent with the delocalized model, implying that f electrons incorporate into these Fermi surface sheets. However, there do not appear to be additional frequencies associated with the α_Z and β_Z sheets of the delocalized model, and orbit β_2 increases as a function of tilt angle away from [001] (Fig. 2C), further suggesting that the β cylinder is fully connected in better qualitative agreement with the localized model. In the Sn-substituted sample, the sizes of the α and β cylinders change slightly compared with their sizes in pure $CeCoIn_5$ (Table 1). In addition, an oscillation of ~16 kT appears for two field angles near [001]. This oscillation does not appear to be harmonically related to the α_{1-3} branches, and its frequency and angle dependence are consistent with a predicted orbit on α_Z of our delocalized model calculations. Furthermore, 1.2- and 2-kT frequencies for field angles near [001] are indicative of holes in the β cylinder (Fig. 2A), and a branch of the β_2 cylinder orbit appears to decrease as a function of tilt angle from [001], in better agreement with the delocalized model (Fig. 1C) and further suggesting that holes develop in the β cylinder. Finally, possible low-frequency oscillations <800 T at several angles, which seem to be present in pure $CeCoIn_5$ over certain angular ranges as well, are most naturally assigned to small γ ellipsoids (Fig. 2C) but could also originate from the γ_Z sheet. Table 1 summarizes the frequency assignments based on comparison to DFT calculations, suggesting that the α_Z and β_Z sheets are present in the Fermi surface of the Sn-substituted sample. From dHvA, it is not possible to conclusively say whether these sheets are absent in pure $CeCoIn_5$ at low temperature because the orbit frequencies on α_Z and β_Z are sensitive to the precise structure of these Fermi surfaces. Nevertheless, the comparison provided in Table 1 is indicative of a Fermi surface reconstruction induced by Sn substitution.

Our ARPES measurements corroborate the dHvA evidence for a Fermi surface reconstruction. Figure 3 compares Fermi surface maps at the Brillouin zone top in pure $CeCoIn_5$ and 3% Sn-substituted $CeCoIn_5$ at 10 K [additional

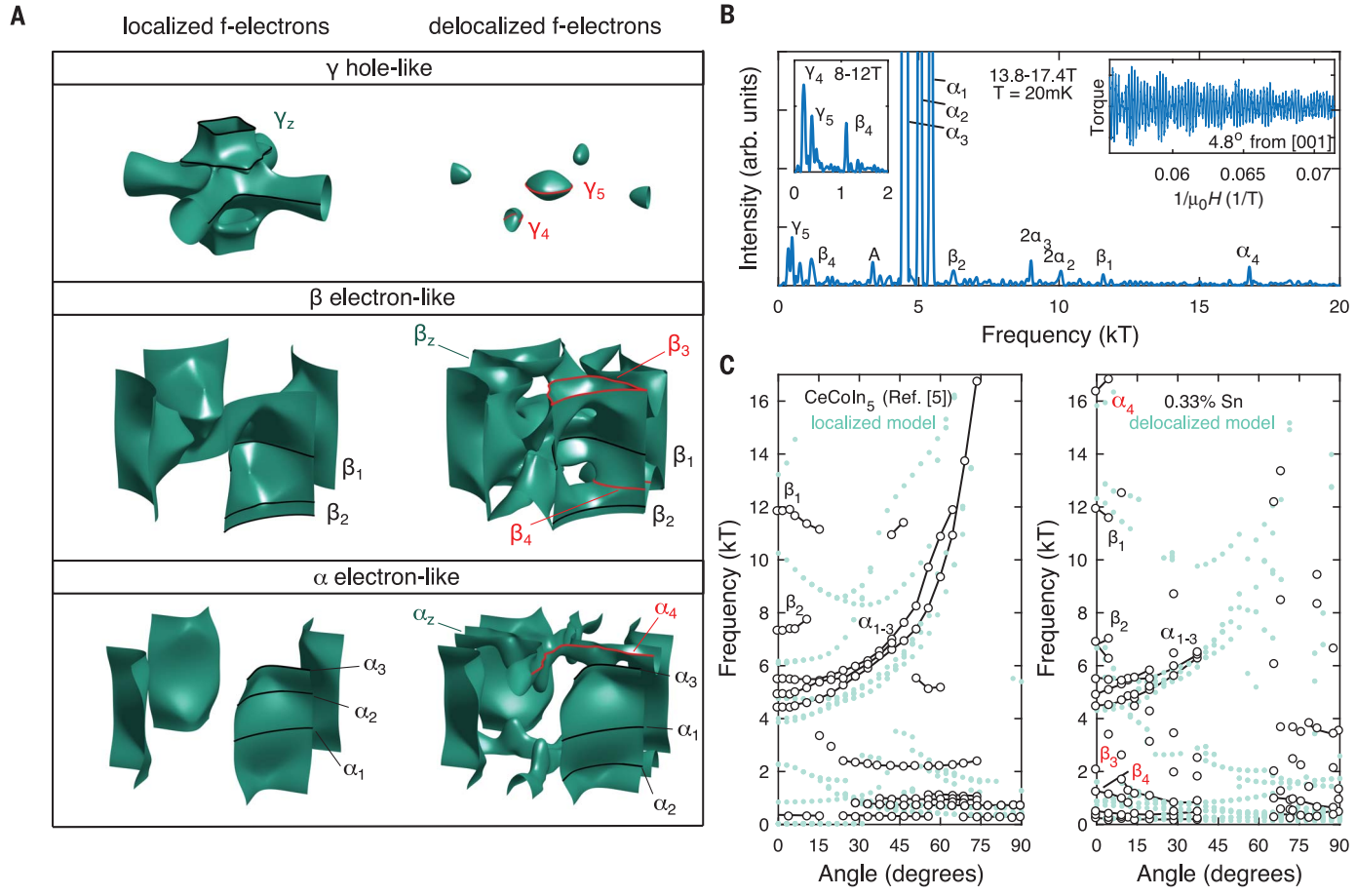

Fig. 2. De Haas–van Alphen oscillations in Sn-doped $CeCoIn_5$ and comparison to DFT calculations. (**A**) DFT-calculated Fermi surface sheets of $CeCoIn_5$ with localized and delocalized f-electron models. Predicted dHvA orbits for $H \parallel [001]$ are drawn in black and red; red orbits are specific to the delocalized f-electron model. (**B**) Characteristic dHvA spectrum with the magnetic field 4.8° away from [001] of a crystal of 0.33% Sn-doped $CeCoIn_5$. The right inset shows oscillations in the magnetic torque after background subtraction. (**C**) dHvA oscillation frequencies as a function of the angle that tilts the magnetic field from the crystallographic [001] to [100] directions in pure $CeCoIn_5$ (*5*) and 0.33% Sn-doped $CeCoIn_5$. Light green points are DFT-calculated frequencies of the localized and delocalized f-electron models, respectively.

data are provided in section 9 of (*21*)]. Our data on pure $CeCoIn_5$ agree well with earlier reports. The cylindrical Fermi surfaces centered at the zone corners are visible. Bright spots near the Z point are probably signatures of the γ_Z Fermi surface, as discussed previously (*27*, *31*). In the 3% Sn-substituted sample, we observed enhanced intensity at the R point of the Brillouin zone relative to the pure material, as well as a qualitative change in structure near the Z point. Overall, the electronic structure appears to change with Sn substitution, with a sharp cross-shaped structure emerging in the RZA plane, which resembles α_Z or β_Z of our delocalized model calculations (α and β bands nearly overlap along this cut; as such, they may be difficult to distinguish from one another in ARPES). Weak features appear at the R point in pure $CeCoIn_5$ as well, potentially indicating that incoherent states exist at the R point—these states may exist because of the partially delocalized f-electron character in the pure material. In Fig. 3C, we explore the temperature dependence of these Fermi surface sheets via the ARPES intensity at the R point. The relative intensity at R increases in the Sn-substituted sample when the temperature decreases below ~90 K with the onset of f/conduction hybridization (fig. S16). In the pure material, the R point spectral weight is relatively constant down to 10 K. This comparison suggests that the Fermi surface sheet in 3% Sn-doped $CeCoIn_5$ emerges, or is made relatively more coherent, because of enhanced f/conduction electron hybridization induced by Sn substitution.

One way to view f-electron delocalization is as a result of Kondo hybridization between the f level and conduction electrons. Although there are reports of hybridization developing below ~45 K in pure $CeCoIn_5$ (*27*) and Cd-doped $CeCoIn_5$ (*32*), resulting in a detectable f-electron contribution to the Fermi surface, we find that the low-temperature carrier density of these materials is consistent with predominantly localized f electrons (Fig. 1). In contrast to that of the pure material, the net carrier density of Sn-substituted samples appears to include the f electrons (Fig. 1C). This change coincides with signatures of new Fermi surface sheets (Fig. 3 and Table 1), which seem to agree well with predicted Fermi surfaces that are specific to the delocalized f-electron DFT model (Fig. 2A). Taken together, these data suggest that Sn substitution of $CeCoIn_5$ induces a Fermi volume–changing transition between a phase with predominantly localized f electrons to one with a delocalized character. This transition could be attributed to an enhancement of the Kondo coupling induced by electron doping (*25*, *33*, *34*). High magnetic fields may compete with the Kondo coupling by polarizing the f electrons, but notably the Hall resistivity remains linear up to 73 T (Fig. 1B), so it seems likely that higher fields are required to induce a complete breakdown of Kondo hybridization.

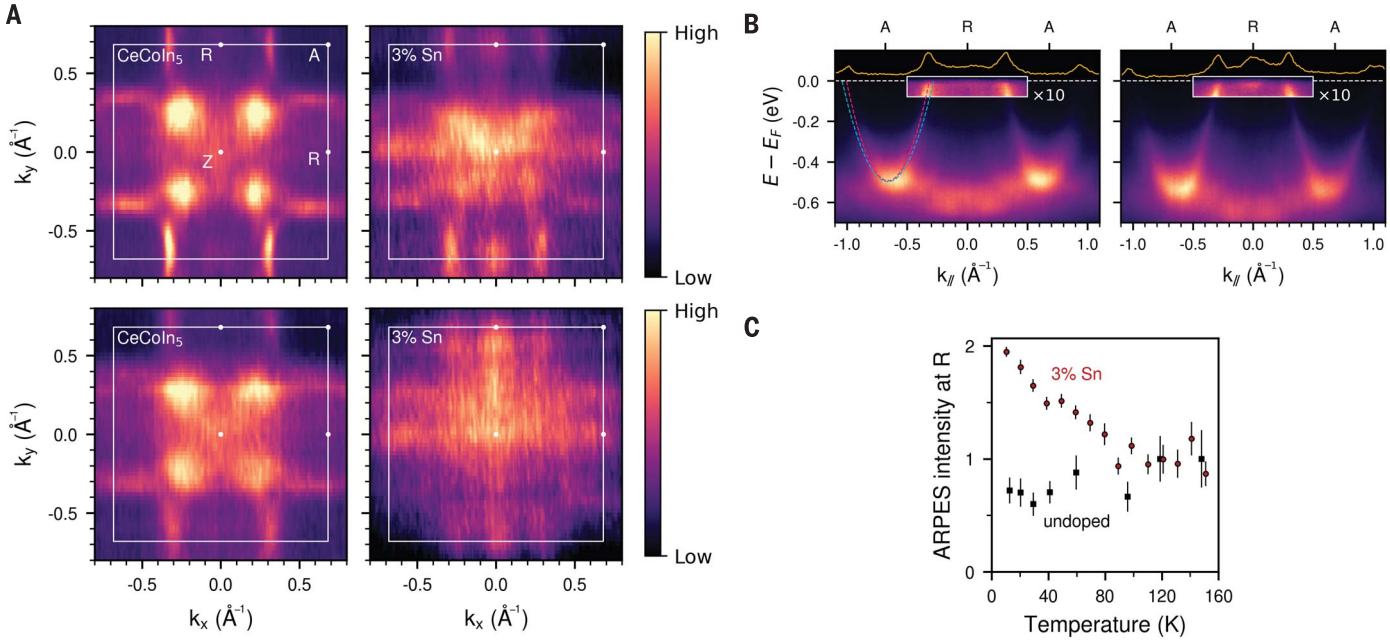

Fig. 3. ARPES measurements of $CeCoIn_5$ and Sn-doped $CeCoIn_5$. (**A**) Fermi surface maps in pure and 3% Sn-substituted $CeCoIn_5$ at the Brillouin zone top (RZA plane). A new Fermi surface sheet appears at the zone top in the Sn-substituted sample. Each of the four subpanels represents measurements on a different cleave. (**B**) A-R-A dispersion cuts. Parabolic α and β bands are labeled by red and blue dotted lines, respectively. The new Fermi surface in the Sn-substituted sample is observed as an increase in spectral intensity at the Fermi level at R. The spectral intensity within the white box has been enhanced by a factor of 10 for clarity. E is the energy, E_F is the Fermi energy, and $E - E_F$ denotes the energy relative to the Fermi energy. (**C**) Comparison of temperature-dependent intensity at the R point normalized to the average value between 120 and 160 K. Error bars indicate estimates of the standard error of the intensity in the fits to the spectral feature at R shown in fig. S15 and an additional 100% margin.

Table 1. De Haas–van Alphen extremal orbit assignments. Values are given in units of kilotesla, $H \parallel [001]$, as determined from experiments and DFT calculations. Each orbit is labeled according to the assigned Fermi surface sheet (orbits are visualized on the calculated Fermi surface sheets in Fig. 2A). Values in parentheses are low-frequency orbits that are consistent in size with the gamma ellipsoids but are not present at all angles as expected for ellipsoidal pockets. –, not present.

Fermi surface	dHvA orbit label	Localized f-electron model	$CeCoIn_5$ (5)	0.33% Sn-doped $CeCoIn_5$	Delocalized f-electron model
γ_Z	γ_1	0.8	–	–	–
γ_Z	γ_2	2.3	–	–	–
γ Cross	γ_3	13.2	–	–	–
γ Ellipsoid	γ_4	–	–	(0.46)	0.7
γ Ellipsoid	γ_5	–	(0.24)	(0.2)	0.22
α Cylinder	α_1	4.8	5.6	5.4	5.6
α Cylinder	α_2	4.0	4.5	4.8	4.4
α Cylinder	α_3	3.9	4.2	4.4	4.3
α_Z	α_4	–	–	16.3	15.8
β Cylinder	β_1	10.3	12.0	11.9	12.3
β Cylinder	β_2	6.1	7.5	6.8	6.7
β_Z/cylinder	β_3	–	–	2.0	1.6
β_Z/cylinder	β_4	–	–	1.2	0.9

A delocalization transition is a reasonable scenario from the perspective of doping-tuned Kondo coupling. Because of the constraints imposed by Luttinger's theorem, the reduction in Fermi volume in the more localized f-electron regime is expected to coincide with antiferromagnetic order where the Brillouin zone is reduced (*15*). It is, however, difficult to reconcile this scenario with the data because the transition to antiferromagnetism is seen only around a Cd doping of 0.6% (*23*), considerably removed from the suggested delocalization transition induced by Sn substitution (Fig. 1C). Furthermore, magnetic order has never been observed in native $CeCoIn_5$ or Sn-substituted $CeCoIn_5$ (*6*, *25*, *33*, *34*), and the ARPES and dHvA data suggest that the Brillouin zone is essentially unchanged by Sn substitution. An alternative possibility is the formation of a fractionalized phase in the more localized f-electron regime (*11*). In this theoretically predicted phase, the f-electron charge localizes to the Ce site, reducing the Fermi volume, whereas the spin excitations of the f moments

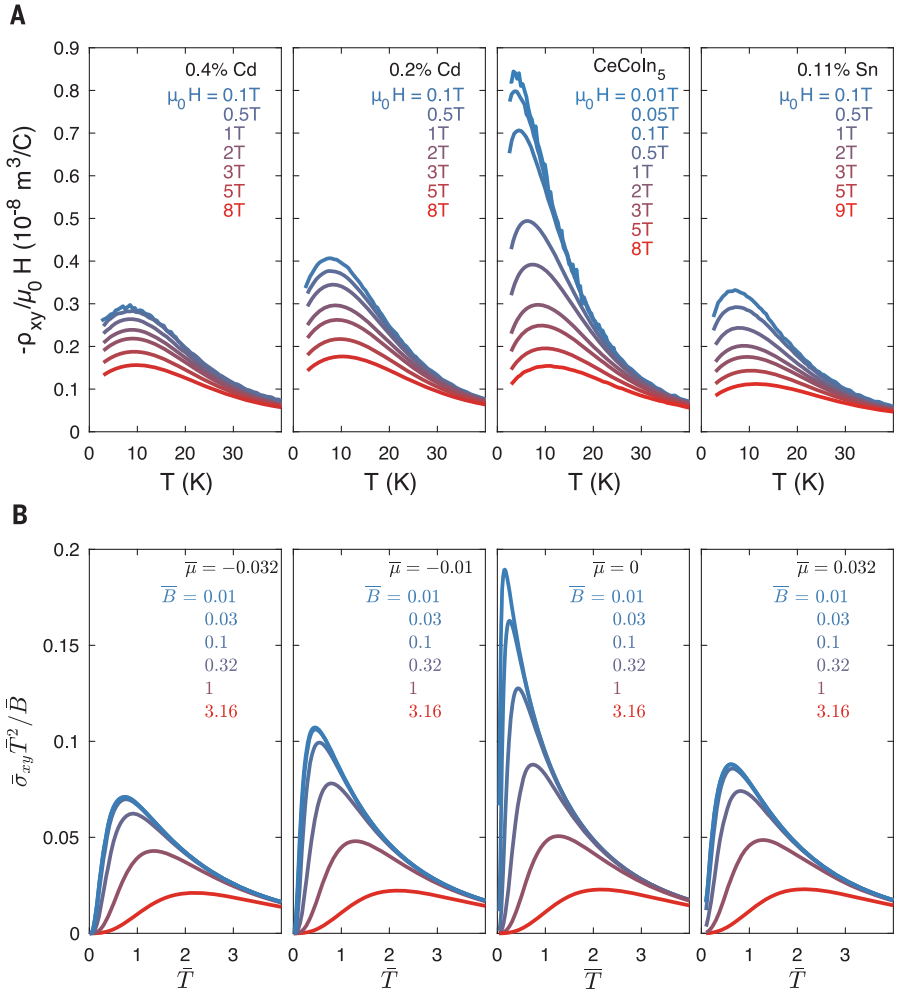

Fig. 4. Comparison of experimental data and theoretical calculations of the conductivity of critical valence fluctuations around an f-electron delocalization transition. (**A**) Experimentally measured Hall resistivity, divided by the applied magnetic field, for samples with different compositions. (**B**) Theoretically predicted Hall effect from bosonic valence fluctuations of the fractionalized Fermi liquid model. Each panel is labeled by the chemical potential in the theory corresponding to the doping level in the experiment, where $\mu < 0$ corresponds to hole doping and $\mu > 0$ corresponds to electron doping. Curves are labeled by the normalized magnetic field value, and all theory data include a parametrization of impurity scattering, $\bar{C} = 4$. See section 7 of (*21*) for the details of the calculation and relevant parameter normalizations.

remain itinerant and form a charge-neutral Fermi surface (*11*). We can speculate that the specific heat remains constant across the substitution series (Fig. 1C) owing to the presence of such a neutral Fermi surface, which conserves the fermionic degrees of freedom of the system even when the density of itinerant electrons appears to increase. One may also expect quantum fluctuations associated with a delocalization transition to enhance the specific heat coefficient. Such an enhancement has been observed as a function of decreasing temperature below 2 K in pure $CeCoIn_5$ (*2*). The confinement of these effects to <2 K temperatures could explain why we do not detect singular behavior in heat capacity (C)/temperature (T) at 4 K across the substitution series.

Our calculations of the Hall conductivity of such a fractionalized phase capture several distinctive aspects of the low-field Hall coefficient in this material. In the simplest description of the fractionalized Fermi liquid, the f electron separates into a fermionic spinon carrying its spin and a gapped bosonic mode, in this case a valence fluctuation, carrying its charge. Delocalization of f electrons can be identified with the closing of the boson gap. Near this transition, the electrical conductivity has contributions from the fermionic spinons, the charged bosons, and the conduction electrons. The spinon and the bosons should be added in series (*35*). The bosons' resistivity will then dominate, owing to their much smaller number, and we therefore neglect the spinon contribution. Adding to this the resistivity of the conduction band in parallel gives

$$R_{\mathrm{H}} = R_{\mathrm{H}}^{c}\frac{\sigma_{\mathrm{c}}^{2}}{(\sigma_{\mathrm{tot}})^{2}} + \frac{1}{\mu_0 H}\frac{\sigma_{xy}^{b}}{(\sigma_{\mathrm{tot}})^{2}} \qquad (2)$$

where σ_{c} and R_{H}^{c} are the longitudinal conductivity and Hall coefficient of the conduction electrons, respectively; σ_{xy}^{b} is the Hall conductivity of the bosonic valence fluctuations; and σ_{tot} is the total conductivity. In our calculation, we consider two processes that contribute to the scattering rate of the valence fluctuations. One process is provided by the internal gauge field (*11*). The other mechanism is scattering on the doped ions, which grows linearly with the doping level (fig. S5). One may expect an enhancement of the low-field Hall coefficient stemming from the second term in Eq. 2, caused by the singular behavior of the valence fluctuations when the boson gap closes. This expectation is corroborated by a semiclassical Boltzmann analysis, the details of which are given in section 7 of (*21*). As shown in Fig. 4, the results of the calculation of the conductivity in this model are in good agreement with the measured Hall coefficient as a function of temperature, doping level, and magnetic field, with the assumption that pure $CeCoIn_5$ is the sample closest to the delocalization transition. The results shown in Fig. 4B are obtained from a calculation of σ_{xy}^{b} and are converted to a Hall coefficient using the physical resistivity of the system $1/\sigma_{\mathrm{tot}} = \rho_{xx} \sim T$, as observed in the experiment over the relevant temperature range. A more complete description of the longitudinal resistivity in this model will be the subject of future work.

We emphasize that the experimental observations illustrated in Fig. 4 are difficult to reconcile with more conventional transport models. From the point of view of band theory, the low-field R_{H} is proportional to the carrier density of the most-mobile carriers (*20*), so it is surprising that R_{H} has such a strong temperature dependence with a peak at finite temperature and retains the same sign and uniformly decreases with either hole or electron doping. In addition, the observed symmetric-in-doping Hall coefficient cannot be readily attributed to disorder scattering induced by substitution, as we find that disordering the material by other means, substituting La for Ce, has a relatively small effect on the low-field R_{H} (fig. S6). These key features of the experimental transport data are captured by the valence fluctuation model described above.

The present study provides evidence that $CeCoIn_5$ exists near a QPT associated with the delocalization of f-electron charge. The absence of evidence for symmetry breaking around this transition opens the possibility

for the fractionalization of f electrons into separate spin and charge degrees of freedom. Although our conductivity calculations support this theoretical picture, direct evidence for such fractionalized electrons is desirable and may be possible with inelastic neutron measurements (*36*) or Josephson tunneling experiments (*37*). On a final note, recent experiments on cuprate high-temperature superconductors find evidence for a Fermi surface reconstruction in which the localized charge of the Mott insulator gradually delocalizes over a certain oxygen doping range near the end point of the pseudogap phase [sometimes referred to as a p to $1 + p$ transition, where p denotes the doped hole concentration (*38*)]. We have presented evidence for an analogous transition in an f-electron metal. It is possible that such a QPT underlies some of the similarities between $CeCoIn_5$ and cuprate superconductors (*1*–*9*), and perhaps our work may help guide interpretation of these recent results for cuprates.

REFERENCES AND NOTES

1. C. Petrovic *et al*., *J. Phys. Condens. Matter* **13**, L337 (2001).
2. A. Bianchi, R. Movshovich, I. Vekhter, P. G. Pagliuso, J. L. Sarrao, *Phys. Rev. Lett.* **91**, 257001 (2003).
3. J. Paglione *et al*., *Phys. Rev. Lett.* **91**, 246405 (2003).
4. Y. Nakajima *et al*., *Phys. C* **460-462**, 680–681 (2007).
5. R. Settai *et al*., *J. Phys. Condens. Matter* **13**, L627 (2001).
6. Y. Kohori *et al*., *Phys. Rev. B* **64**, 134526 (2001).
7. V. A. Sidorov *et al*., *Phys. Rev. Lett.* **89**, 157004 (2002).
8. B. B. Zhou *et al*., *Nat. Phys.* **9**, 474–479 (2013).
9. C. Stock, C. Broholm, J. Hudis, H. J. Kang, C. Petrovic, *Phys. Rev. Lett.* **100**, 087001 (2008).
10. Y. Tokiwa, E. D. Bauer, P. Gegenwart, *Phys. Rev. Lett.* **111**, 107003 (2013).
11. T. Senthil, M. Vojta, S. Sachdev, *Phys. Rev. B* **69**, 035111 (2004).
12. C. M. Varma, *Phys. Rev. B* **73**, 155113 (2006).
13. S. Lederer, Y. Schattner, E. Berg, S. A. Kivelson, *Proc. Natl. Acad. Sci. U.S.A.* **114**, 4905–4910 (2017).
14. M. Oshikawa, *Phys. Rev. Lett.* **84**, 3370–3373 (2000).
15. Q. Si, F. Steglich, *Science* **329**, 1161–1166 (2010).
16. S. Paschen *et al*., *Nature* **432**, 881–885 (2004).
17. A. Schröder *et al*., *Nature* **407**, 351–355 (2000).
18. P. Gegenwart *et al*., *Phys. Rev. Lett.* **81**, 1501–1504 (1998).
19. J. Custers *et al*., *Nature* **424**, 524–527 (2003).
20. A. B. Pippard, *Magnetoresistance in Metals* (Cambridge Univ. Press, 2009).
21. Supplementary materials.
22. S. Singh *et al*., *Phys. Rev. Lett.* **98**, 057001 (2007).
23. L. D. Pham, T. Park, S. Maquilon, J. D. Thompson, Z. Fisk, *Phys. Rev. Lett.* **97**, 056404 (2006).
24. Q. Y. Chen *et al*., *Phys. Rev. B* **100**, 035117 (2019).
25. K. Chen *et al*., *Phys. Rev. B* **97**, 045134 (2018).
26. A. Koitzsch *et al*., *Phys. Rev. B* **77**, 155128 (2008).
27. S. Jang *et al*., *Proc. Natl. Acad. Sci. U.S.A.* **117**, 23467–23476 (2020).
28. N. Gauthier *et al*., *Phys. Rev. B* **102**, 125111 (2020).
29. N. J. Curro *et al*., *Phys. Rev. B* **64**, 180514(R) (2001).
30. S. Fujimori, *J. Phys. Condens. Matter* **28**, 153002 (2016).
31. Q. Y. Chen *et al*., *Phys. Rev. B* **96**, 045107 (2017).
32. Q. Y. Chen *et al*., *Phys. Rev. B* **100**, 235148 (2019).
33. K. Gofryk *et al*., *Phys. Rev. Lett.* **109**, 186402 (2012).
34. H. Sakai *et al*., *Phys. Rev. B* **92**, 121105 (2015).
35. L. B. Ioffe, A. I. Larkin, *Phys. Rev. B* **39**, 8988–8999 (1989).
36. A. Banerjee *et al*., *NPJ Quant. Mater.* **3**, 8 (2018).
37. T. Senthil, M. P. A. Fisher, *Phys. Rev. B* **64**, 214511 (2001).
38. S. Badoux *et al*., *Nature* **531**, 210–214 (2016).
39. N. Maksimovic, J. Rusz, T. Cookmeyer, D. Eilbott, J. Gobbo, Ce115, OSF (2021).

ACKNOWLEDGMENTS

We thank C. Varma, S. Sachdev, S. Chatterjee, M. Vojta, and J. D. Denlinger for helpful discussions and E. Green for support during experiments at the millikelvin facility at the National High Magnetic Field Laboratory. Hall bar devices were fabricated at the Focused Ion Beam at the National Center for Electron Microscopy Sciences at Lawrence Berkeley National Laboratory. **Funding:** This work was supported by the U.S. Department of Energy, Office of Science, Basic Energy Sciences, Materials Sciences and Engineering Division under contract DE-AC02-05-CH11231 within the Quantum Materials program (KC2202). V.N., T.C., and D.H.E. are supported by National Science Foundation Graduate Research Fellowship grant DGE-1752814. This work was partially supported by the Gordon and Betty Moore Foundations EPiQS Initiative through grant GBMF9067. P.M.O. and J.R. are supported by the Swedish Research Council (VR) and K. and A. Wallenberg Foundation award 2015.0060. DFT calculations were performed using resources of Swedish National Infrastructure for Computing (SNIC) at the NSC center (cluster Tetralith). Pulsed-field and dilution fridge experiments were conducted at the National High Magnetic Field Laboratory facilities in Tallahassee, Florida, and Los Alamos, New Mexico, respectively, which are supported by National Science Foundation Cooperative Agreement DMR-1644779 and the state of Florida. **Author contributions:** N.M., I.M.H., and F.W. performed continuous field Hall effect measurements. N.M. and V.N. performed the quantum oscillation experiments. N.M., S.F., F.W., S.J., and A.G. grew the samples and performed heat capacity and magnetization measurements. T.C., Y.W., and E.A. performed theoretical calculations of the Hall coefficient. J.R. and P.M.O. performed DFT simulations of Fermi surface topologies and dHvA oscillation frequencies. S.C.H. and E.M. fabricated Hall bar devices for pulsed-field measurements. A.B. performed dilution fridge measurements. J.S., J.C.P., L.W., and R.M. performed pulsed-field measurements. D.H.E., P.A., Y.L., S.C., and J.G. performed ARPES measurements. All authors contributed to writing the manuscript. **Competing interests:** The authors declare no competing interests, financial or otherwise. **Data and materials availability:** All data provided in this report are publicly available at the Open Science Framework (*39*).

SUPPLEMENTARY MATERIALS

science.org/doi/10.1126/science.aaz4566
Materials and Methods
Supplementary Text
Figs. S1 to S16
References (*40*–*44*)

10 September 2019; resubmitted 18 June 2020
Accepted 15 November 2021
Published online 2 December 2021
10.1126/science.aaz4566

Evidence for a delocalization quantum phase transition without symmetry breaking in CeCoIn

Nikola MaksimovicDaniel H. EilbottTessa CookmeyerFanghui WanJan RuszVikram NagarajanShannon C. HaleyEran ManivAmanda GongStefano FaubelIan M. HayesAli BanguraJohn SingletonJohanna C. PalmstromLaurel WinterRoss McDonaldSooyoung JangPing AiYi LinSamuel CiocysJacob GobboYochai WermanPeter M. OppeneerEhud AltmanAlessandra LanzaraJames G. Analytis

Science, 375 (6576), • DOI: 10.1126/science.aaz4566

A gentle reconstruction

Changes in the volume of a material's Fermi surface are typically associated with the breaking of symmetry. Maksimovic *et al*. found evidence for an unusual type of this Fermi surface reconstruction, one without symmetry breaking, in the heavy fermion compound cerium cobalt indium (CeCoIn). Doping the material with tin led to abrupt changes in Hall effect, quantum oscillation, and photoemission signals. The researchers interpret the findings in terms of the delocalization of f-electrons associated with cerium atoms. —JS